Carbohydrate Polymers 277 (2022) 118815

Contents lists available at ScienceDirect

Carbohydrate Polymers

journal homepage: www.elsevier.com/locate/carbpol

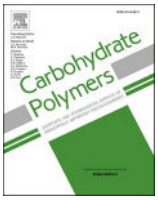

Chitosan nanoparticles loaded with garlic essential oil: A new alternative to tebuconazole as seed dressing agent

Maria Mondéjar-López [a,1], Angela Rubio-Moraga [a,b], Alberto José López-Jimenez [a,b], Joaquin C. García Martínez [c,d], Oussama Ahrazem [a,b], Lourdes Gómez-Gómez [a], Enrique Niza [a,*]

[a] *Instituto Botánico, Departamento de Ciencia y Tecnología Agroforestal y Genética. Universidad de Castilla-La Mancha, Campus Universitario s/n, 02071 Albacete, Spain*

[b] *Escuela Técnica Superior deIngenieros Agrónomos y Montes, Departamento de Ciencia y Tecnología Agroforestal y Genética, Universidad de Castilla-La Mancha, Campus Universitario s/n, 02071 Albacete, Spain*

[c] *Universidad de Castilla-La Mancha, Departamento de Química Inorgánica, Orgánica y Bioquímica, Facultad de Farmacia, C/ José María Sánchez Ibáñez s/n, 02008 Albacete, Spain*

[d] *Universidad de Castilla-La Mancha, Regional Center for Biomedical Research (CRIB), C/ Almansa 13, 02008 Albacete, Spain*

ARTICLE INFO

Keywords:
Garlic essential oil
Polysaccharides
Chitosan
Nanotechnology
Biotechnology
Fungicide
Crop control

ABSTRACT

In this study, garlic essential oil (GEO) has been encapsulated in chitosan nanoparticles (NPCH) with sodium tripolyphosphate (TPP). Fourier transform infrared (FT-IR) spectroscopy, UV–vis spectrophotometry, thermogravimetric analysis (TGA) and X-ray diffraction (XRD) techniques were applied to characterize GEO-NPCH. The obtained nanoparticles exhibited a regular distribution and spherical shape with size range of 200–400 nm as revealed by scanning electron microscopy (SEM). The maximum encapsulation efficiency (EE) and loading capacity (LC) of GEO-loaded chitosan nanoparticles were about 32.8% and 19.8% respectively. Nanoparticle formulations of GEO were found to have antifungal activity against *Aspergillus versicolor*, *A. niger* and *Fusarium oxysporum*. In addition, they showed growth promoting effects by increasing emergence, shoot and root fresh weight on wheat, oat and barley.

1. Introduction

Diseases caused by soil pathogenic fungi are the cause of severe losses in agrarian production and a threat for food safety (Fisher et al., 2012). Antifungal agents have greatly contributed to the protection of agricultural crops, leading to an increase in agricultural productivity. However, growing global population, global warming and rise in fungal resistance entail new challenges for the agricultural sector, leading to the necessity of efficient and green fungicides.

Currently, triazoles are the most used antifungals due to their high efficiency and broad-spectrum activity. Among this family, Tebuconazole (TB) is an effective systemic fungicide that has been widely used in both agricultural and medical sectors for the control of fungal diseases, and is the main antifungal utilized nowadays as seed dressing in different cereals (Marín et al., 2013). However, the extensive practice of TB and other triazoles in agriculture has raised concerns about their environmental repercussions, as well as the risks derived due to their toxicological effects and the emergence of antifungal-resistant strains of pathogenic fungi (Brauer et al., 2019) (Lopez-Antia et al., 2021). Therefore, it is important to develop alternative strategies to TB treatment, combining ecological compounds with antifungal activity as well as elicitors that enhance the plant defenses against fungal attack.

Essential oils (Eos) and terpenes arise as natural antifungal, antimicrobial and antioxidant agents (D'agostino et al., 2019; Mahizan et al., 2019; Valdivieso-Ugarte et al., 2019). Some Eos and terpenes can act as antifungals through different mechanisms such as membrane/wall destabilizers, by inhibition of efflux pump, acting against fungal mitochondria or producing Reactive oxygen species (ROS), etc. (Nazzaro, 2017). Among these compounds, *Allium sativum* L. essential oil is mainly composed by allyl disulfide, allyl trisulfide, allyl (E)-1-propenyl disulfide, allyl methyl trisulfide, and diallyl tetrasulfide (Thuy et al., 2020). These sulphured compounds interact with hydrogen sulfide groups of the cell and can form disulfide bonds displaying antifungal activity against different fungus species such as *Aspergillus niger, Penicillium*

* Corresponding author.
E-mail address: enrique.niza@uclm.es (E. Niza).
[1] First author.

https://doi.org/10.1016/j.carbpol.2021.118815
Received 20 August 2021; Received in revised form 9 October 2021; Accepted 24 October 2021
Available online 27 October 2021

cyclopium and *Fusarium oxysporum* among others (Benkeblia, 2004) (Somrani et al., 2020).

Despite their promising properties, EOs and terpene applications remain hampered by their high volatility, low solubility in water and instability against light and oxygen environments (Niza et al., 2020). Encapsulation of these bioactive compounds is an effective approach to protect them against degradation under adverse environmental conditions.

Chitosan (CH) is a linear copolymer composed of β-(1–4) linked D-glucosamine and *N*-acetyl-D-glucosamine units and is currently drawing attention as a promising raw material in pharmaceutical, medicinal, and crop control applications (Hosseinnejad & Mahdi, 2016). It is commonly used in crop control and agriculture against plant diseases, and has been shown to display toxicity against a broad spectrum of fungi, inhibiting both growth and development (Muzzarelli et al., 2001). Moreover, this cationic polysaccharide has huge promising applications in nanotechnology due to its controllable and easy extraction, biocompatibility, biodegradability, non-toxicity, antifungal properties, easy chemical modification in addition to, its ability to form gels, films and solid nanoparticles (Ashra et al., 2019; Hu & Luo, 2016; Keawchaoon & Yoksan, 2011). The versatility of this polymer and the antifungal properties of chitosan have been used to improve the stability and enhance the fungicidal properties of some EO such as clove essential oil, inhibiting the growth of *Cymbopogon martini* and *Foeniculum vulgare* among others (Hasheminejad, Khodaiyan, Safari, 2019a; Kalagatur et al., 2018; Kumar et al., 2020). Furthermore, oligosaccharides derived from CH have been described as an elicitor leading to a variety of defence responses in host plants against microbial infections, including the accumulation of phytoalexins, pathogen-related proteins (PR) and proteinase inhibitors, lignin synthesis, and callose formation (Hadrami et al., 2010). Additionally, CH has been applied as a foliar treatment agent (Bittelli et al., 2001), as a soil amendment (Rabea et al., 2003), and as a seed coating agent (Kananont et al., 2010; Rabea et al., 2003).

Different encapsulation techniques have been applied to protect EOs and terpenes. Among these techniques, the ionic gelation method was used via nontoxic and multivalent material such as Tripolyphosphate, (TPP) (Hadidi et al., 2020) to encapsule Oregano EO, eugenol, carvacrol, *Mentha spicata* EO, clove EO, and *Satureja hortensis* L. EO, among others (Ashra et al., 2019; Fakhreddin et al., 2013; Feyzioglu & Tornuk, 2016; Hadidi et al., 2020; Hasheminejad, Khodaiyan, Safari, 2019b; Keawchaoon & Yoksan, 2011; Woranuch & Yoksan, 2013). In addition, CH formulations dealing with the production of CH nanoparticles (NPCH) showed promising activities by promoting seed germination and seedling growth in wheat, tomato and other plant species (Li et al., 2019) (Chun & Chandrasekaran, 2019).

Thus, the present study has been designed for a threefold purpose: to evaluate the garlic essential oil (GEO) encapsulation in TPP-NPCH in order to improve its stability; to increase its antifungal activity against several fungi, and to evaluate its efficiency as an antifungal coating agent on different cereal seeds, as an ecofriendly alternative to TB. We also look for the possible elicitor effects on seed germination under controlled and field conditions.

2. Material and methods

2.1. Materials

Low molecular weight chitosan (CH) (50–190 kDa) with 75–85% degree of deacetylation, Tripolyphosphate (TPP), 3-(4 5-dimethylthiazol-2-yl)-2 5-diphenyltetrazolium bromide (MTT), Tebuconazole (TB) and all the solvents were supplied by Sigma-Aldrich (Madrid, Spain). Orius 20 EW (20% of Tebuconazole) by Nufarm Spain and GEO was purchased from Pranarom (Barcelona, Spain). The organisms used for the antifungal assays consisted of species of *Aspergillus versicolor*, *A. niger* and *Fusarium oxysporum*, which were isolated from soil and were examined visually and microscopically for morphological characterization of isolates, as previously described in (Palmero et al., 2014) and their identity confirmed using ITS primers as described in (Gardes et al., 1993).

2.2. Preparation of loaded and unloaded GEO-chitosan nanoparticles

Chitosan nanoparticles (NPCH) were formulated via ionic-gelation method described by (Keawchaoon & Yoksan, 2011) with some modifications. Briefly, CH solution at 0.2% was prepared dissolving CH flakes in acetic acid at 1% under continuous stirring overnight. Then, the CH solution was sonicated 10 min until completely dissolved. 50 mL of CH solution was mixed at 1000 RPM in a 1% Tween 80 solution and heated at 50 °C. Finally, TPP aqueous solution at 0.2% was added dropwise at 2 mL/min under continuous stirring to induce the ionic gelation. Afterwards, agitation was carried out at 700 RPM for 40 min. The nanoparticles were collected after centrifugation at 15,000 RPM for 20 min at 4 °C, and, subsequently, washed several times with mQ water. The nanoparticle suspension was frozen at −80 °C and freeze dried for 48 h at −50 °C (LyoQuest-85/208V 60 Hz, Teslar).

Encapsulation of GEO into chitosan nanoparticles (GEO-NPCH) was formulated in a two-step process: firstly, oil-in-water emulsification (o/w) was carried out, followed by the ionic gelation method as described above. Briefly, 50 mL of previously prepared CH solution was mixed at 1000 RPM in a 1% Tween 80 solution and heated at 50 °C. Subsequently, different amounts of GEO to form four ratios of CH:GEO (1:0, 1:0.25, 1:0.5,1:0.75 and 1:1 w/w) were added dropwise under continuous agitation and emulsified at 1000 RPM during 10 min at room temperature. Finally, TPP aqueous solution at 0.2% was added dropwise at 2 mL/min under continuous stirring to induce the ionic gelation. Afterwards, agitation was carried out at 700 RPM for 40 min. The nanoparticles were collected after centrifugation at 15,000 RPM for 20 min at 4 °C, and, subsequently, washed several times with mQ water. The nanoparticle suspension was frozen at −80 °C and freeze dried for 48 h at −50 °C (LyoQuest-85 / 208 V 60 Hz, Teslar).

2.3. Determination of encapsulation efficiency and loading efficiency of garlic essential oil-chitosan nanoparticles (GEO-NPCH)

A sample suspension (100 μL) was mixed with 5 mL of HCL 2 M and boiled at 95 °C in reflux. After cooling, 1 mL of absolute Ethanol was added to the homogeneous mixture before centrifugation at 9000 rpm for 1 min at 25 °C. The supernatant was analysed by UV–vis spectrophotometry over a wavelength range of 250–400 nm to cover the maximum absorption wavelength of garlic essential oil (325 nm) (Ang et al., 2009). Chitosan nanoparticles without GEO (NPCH) were also prepared as control in the same manner.

Loading capacity (LC) and encapsulation efficiency (EE) of GEO were calculated according to the following equations:

$$LC\% = (\text{weight of encapsulated GEO (mg)})/(\text{weight of total (GEO encapsulated} + \text{scaffold weight) (mg)}) \times 100\%$$

$$EE\% = (\text{weight of encapsulated GEO (mg)})/(\text{weight of GEO feeding (mg)}) \times 100\%$$

2.4. Instrumental characterization of nanoparticles

The particle characterization of nano-formulations (size, zeta potential and polydispersity index (PDI)) was determined by Dynamic light scattering (DLS) using a Zetasizer (3000HSM Malvern Ltd., IESMAT, Spain) with the following specifications: chitosan refractive index (IR) of 1.700, absorption index 0.010 and water solvent RI: 1.33, with a viscosity of 0.8872 cP. Measurements were performed in triplicate.

IR spectra was recorded on an attenuated total reflectance-Fourier transform infrared (ATR–FTIR) spectrophotometer (VARIAN 640-IR with a Pike Diamond/KRS-5 HS Performance Crystal Plate) and the main peaks were given in cm^{-1}. ATR allows us to use the samples directly in solid or liquid state without the need of KBr or lugol's iodine matrix. Specifically, for NPCH and GEO-NPCH, 20 mg nanoparticles were powdered in a mortar, the thin solid was placed on the diamond plate and pressed until a homogeneous pellet was obtained. GEO, being liquid, a drop of approximately 200 μL was placed on the plate and the tip was placed in such a way that the surface tension of the drop covered the diamond plate homogeneously. 256 scans were acquired at an instrument resolution of 1 cm^{-1} over the spectral range between 650 and 4000 cm^{-1} owing to the frequency cutoff of the ATR–FTIR internal reflection element (IRE) used.

The thermal decomposition mechanisms were determined on a thermogravimetric analyser (TGA Q20, TA Instruments) fitted with a standard platinum pan. The differential scanning calorimetry (DSC) experiments were carried out using a DSC Q50 system (TA Instruments) equipped with a standard aluminium pan with 10 °C/min increasing heat rate (30–320 °C) to investigate the thermal stability of pure GEO, NPCH and GEO-NPCH. A sample of indium was used as reference. In all cases, samples of about 3 mg were heated at a 10 °C/ min rate under nitrogen atmosphere.

X-ray diffraction (XDR) patterns of samples were scanned over a 2θ range of 5 to 60° using an X-R diffractometer with a speed angle of 0.05° /min.

Morphological surface and shape analysis of NPCH and GEO-NPCH were studied by Scanning electron microscopy (SEM). Samples were sputtered with Pt and observed with a Jeol 7800 F electron microscope at 20 KV.

2.5. Determination of antifungal activity

Different ratios of CH:GEO (1:0, 1:0.25, 1:0.5 and 1:0.75) were evaluated. For antifungal analysis the GEO-NPCH ratio 1:0.75 was chosen to perform the assay, since this combination resulted in a PDI < 0.7 and higher LC than 1:0.5 and 1:0.25 ratios.

The antifungal assay using spores from *A. versicolor, A. niger* and *F. oxysporum* were performed according to (Rubio-moraga et al., 2013), with some modifications. The treatments were prepared in a sterile Eppendorf tube containing 3000 spores (40 μL) of each fungus in sterile potato dextrose broth (PDB), and 20 μL of the different treatments. The mixture was poured into a hole perforated by using a Pasteur Pipette in the centre of potato dextrose agar (PDA) plates. All plates were incubated at 28 °C for 6 days to evaluate the antifungal index (%) = ((C-T)/C) × 100, and the minimum inhibitory concentrations (MIC) of each treatment, where C and T were radial growth (mm) for the control and for the plates treated with the different fungi.

The antifungal assay after the germination of the spores was performed according to (Rubio-Moraga et al., 2013), with some modifications. The spore suspension at a concentration of 5×10^3 spores/mL (100 μL) was transferred to a 96-well microtiter plate. Plates were incubated 24 h at 28 °C and the treatments were added by using the serial dilution method with a dilution factor of 1/3. Plates were incubated for another 24 h at room temperature and all were treated with 10 μL of 3-(4 5-dimethylthiazol-2-yl)-2 5-diphenyltetrazolium bromide (MTT; 5 mg/mL in PBS; Sigma). Finally, plates were incubated overnight at room temperature, followed by the addition of 100 μL of MTT solvent (0,1 NHCl in anhydrous isopropyl alcohol).

2.6. Evaluation of GEO-chitosan nanoparticles as seed coating agent

To evaluate the germination rate of the different seed coating agents, three batches of 30 g of seeds of wheat (*Triticum vulgare*), oat (*Avena sativa*), and barley (*Hordeum vulgare*), were coated with 3.5 mL of each treatment. 30 g of seeds without treatment, 30 g of seeds treated with NPCH and GEO-NPCH at 2.5 mg/mL and 30 g of seeds treated with TB at commercial doses (9 mg/mL of pure TB) were used. After coating, seeds were dried at room temperature. Batches of 100 seeds of each cereal were placed in sterile wet filter paper and incubated at 25 °C for 5–7 days in a germination chamber with 21.8 °C, short day length with 8 h light and 16 h dark. The effect on seed germination was evaluated by counting the number of survival seeds. The experiment was carried out in triplicate.

To evaluate the morphological effects in plants, batches of 100 g of wheat seeds were treated with NPCH and GEO-NPCH material at different concentrations (7 mg/mL, 2 mg/mL and 1 mg/mL). The effect was compared to the concentration recommended by the manufacturer of TB formulation (45 mg/mL of product with 9 mg/mL of pure TB). Each treatment was tested under field conditions. The seeds were grown in Albacete (Spain) at coordinates: 39°07′06.2"N 1°30′40.8"W. 10 m^2 of the cultivation area was divided into 6 micro-plots for each treatment. A batch of 10 seeds for each treatment was collected 15 days after sown. The seeds were evaluated by measuring weight, root length and leaf length in mm. Three to five biological replicates with three technical replicates per biological replicates were analysed.

2.7. Statistics

The obtained data were statistically analysed using one-way ANOVA and Dunnet's Multiple Comparisons test with the statistical software

Table 1
Average size, Polydispersity (PDI), *Z*-potential, Encapsulation efficiency (EE) and loading capacity (LC) for NPs characterization. Data are expressed as mean ± s.e.m. from at least three independent experiments.

NPs formulation	Average size (d.nm)	PDI	Z-potential (mV)	%EE	%LC
NPCH	172.3 ± 0.71	0.42 ± 0.01	+49.8 ± 0.75	–	–
GEO-NPCH 1:0.25	186.9 ± 0.99	0.46 ± 0.02	+32.6 ± 0.60	32.8 ± 3.50	5.2 ± 1.15
GEO-NPCH 1:0.5	194.1 ± 4.37	0.44 ± 0.01	+31.2 ± 0.57	27.8 ± 0.27	8.7 ± 0.27
GEO-NPCH 1:0.75	352.2 ± 1.95	0.51 ± 0.06	+27.3 ± 0.80	24.7 ± 0.58	10.8 ± 0.40
GEO-NPCH 1:1	253.4 ± 18.58	0.75 ± 0.05	+19.8 ± 0.25	23.8 ± 0.29	19.4 ± 0.98

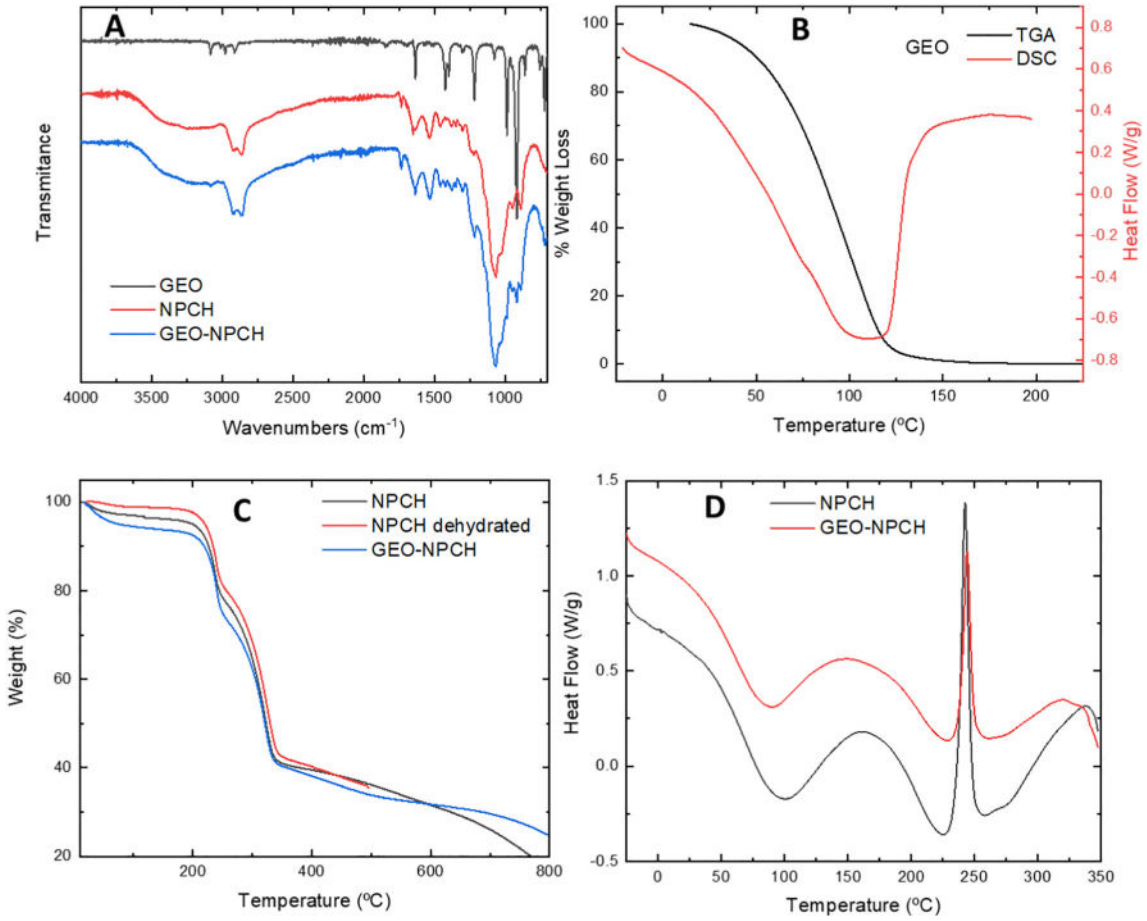

Fig. 1. A) FTIR of GEO, NPCH and GEO-NPCH; B) TGA and DSC of GEO; C) TGA of NPCH, NPCH dehydrated and GEO-NPCH; D) DSC of NPCH and GEO-NPCH.

GraphPad Prism version 5.0.0 for Windows, GraphPad Software, San Diego, California USA. The differences were tested on < 0.05 (95% probability level).

3. Results and discussion

3.1. Size and surface charge of GEO-chitosan nanoparticles

The chitosan backbone can be modified to alter properties such as solubility, mucoadhesion and stability for specific applications. Both the -NH_2 and -OH groups of chitosan are the active sites for modification. As a result of its safe profile, biodegradability, and biocompatibility, chitosan is being used in different fields, e.g. biomedical, pharmaceutical, food, and environmental. To enhance the stability and GEO encapsulation efficiency, GEO-chitosan nanoparticles were obtained using different CH:GEO ratio formulations ranging from 1:0 to 1:1. To determine NP size, Z potential, and polydispersity index (PDI) of each ratio formulations, DLS technique was applied. The results presented in Table 1 showed that NPs ranges from 172 to 352 nm in diameter; while the size of these NPs went up as the amount of GEO was increased. This behaviour has been previously reported in other essential oils such as clove oil. Authors described that the increase of clove oil incorporation in the formulation increased NP size from 265 nm (ratio 1:0.25) up to 445 nm (ratio 1:1) (Hadidi et al., 2020). *Mentha piperita* essential oil encapsulated in chitosan nanogel showed a size increase from 567 nm to 576 nm after essential oil incorporation (Ashra et al., 2019). Tavassoli et al. formulated nanoparticles from chitosan nanofibers by TPP cross-linking encapsulating Quercetin and lactoferrin, reaching a size range between 87.5 and 200.3 nm (Tavassoli et al., 2021). The PDI showed the same pattern in comparison to the pattern of size of NPs, the PDI index of the NPs was higher as the amount of GEO was increased and went from 0.4 in 1:0.25 to 0.7 in 1:1, confirming that formulations are monodisperse and stable. Meanwhile, the CH:GEO ratio formulation 1:1 showed a PDI value >0.7, indicating a very broad particle size distribution (Danaei et al., 2018).

All formulations assayed presented a positive surface charge with an interval ranging from +19.8 to +49.8 mV, which is in accordance with previous studies regarding chitosan NPs encapsulating different active molecules. These positive charges arise from the protonation of amino groups. Other formulations encapsulating GEO, such as the liposomes described by Kamkar et al., showed negative charges (−7.23 mV) due to the use of non-cationic lipids in their formulation (Kamkar et al., 2021). A different formulation of Simvastatin encapsulated into chitosan nanoparticles showed the same trend and a positive surface charge extending from +16 to +45 mV (Delan et al., 2020) was also observed. Likewise, a study conducted by Woranuch et al. described that surface charge of chitosan nanoparticles after Eugenol encapsulation has a positive charge going from +16 to +34 mV (Woranuch & Yoksan, 2013). Studies with Thymol encapsulated in chitosan nanoparticles showed a positive surface charge in all different ratios of chitosan, surfactant, terpene and also with temperature changes (Çakır et al., 2020). The positive surface charge decreases with the increase of GEO size into NPs due to GEO interaction with NPs, producing changes in the structure and charge. In addition, Z potential results confirm that NPCH and GEO-NPCH 1:0.25, 1:0.5, and 1:0.75 have a high stability, as shown in Table 1, while the 1:1 CH:GEO ratio presents a more unstable formulation − + 19.8 mV, which matches with the PDI value-. Some research groups have reported that CH nanoparticles became enlarged and their zeta potential value went down when drugs were incorporated (Keawchaoon & Yoksan, 2011). They also found that increased drug content

reduced zeta potential value.

3.2. Encapsulation efficiency and loading efficiency

In order to measure the GEO content in NPs formulations, spectrophotometry analysis at 325 nm wavelength was carried out. The results, shown in Table 1, indicated that EE% decreased and LC% increased with GEO amounts used in these formulations. These findings seem to be in accordance with previous studies for other oils such as oregano, which ranged from 25% and 1% to 6% and 2% of EE% and LC%, respectively (Fakhreddin et al., 2013), *Coriandrum sativum* encapsulated in Chitosan nanoparticles showed a decrease from 76% to 41% of EE% with the increase of essential oil with respect to chitosan (1:0.6 to 1:1) (Das et al., 2019), while in *Cinnamomun zeylanicum* the decrease of EE% went from 20% to 10% as the amount of essential oil was increased in the formulation (Matshetshe et al., 2018). GEO-NPCH shows a high LC%, with values reaching up to 19.4% as maximum ratio. Previous studies with clove oil-chitosan NPs have reached 6.2 LC% in 1:1 CH:EO maximum ratio (Hasheminejad, Khodaiyan, Safari, 2019b). Other studies using clove oil achieved an EE% of clove essential oil of 73.4%, although data from LC% are missing (Hadidi et al., 2020). Data from encapsulation of Eugenol into chitosan NPs reached EE% and LC% values of 20.2% and 12.8% respectively (Woranuch & Yoksan, 2013). The above results suggested that nanoparticles increased when the initial content of active substances went up, while further increased concentration resulted in EE reduction.

3.3. Chemical structure of GEO-chitosan nanoparticles

The chemical composition was determined by identification of the principal functional groups through FT-IR technique. The attenuated total reflectance (ATR) accessory allowed us to identify the main functional groups present directly from the nanoparticles or essential oil without the need to use matrices. FTIR is typically employed to investigate the interaction between functional groups. However, the technique allows us to verify the existence of functional groups whose vibrational modes are characteristic. In our case, it is possible to see bands of functional groups associated with GEO in the nanoparticles with the essence that are not present in the nanoparticles without essential oil. FT-IR spectra of GEO, NPCH and GEO-NPCH are shown in Fig. 1. NPCH and GEO-NPCH spectra were very similar since their content was mainly chitosan. A broad band between 3750 cm^{-1} and 2500 cm^{-1}, associated with the stretch of the O—H and N—H bonds, was clearly observed. As shown in the gravimetric analysis, chitosan nanoparticles were hygroscopic and had a great tendency to absorb water. This signal includes both chitosan O—H structure and water in its different strengths due to the hydrogen bonds formed. From the spectra, additional characteristic peaks of chitosan were observed at 2916 cm^{-1} and 2864 cm^{-1} due to C—H bond stretching of sp^3 carbon, 1634 cm^{-1} due to carbonyl stretching C═O of the amide, 1533 cm^{-1} due to N—H bending of the chitosan, and 1066 cm^{-1} due to the tension of the different C—O bonds (Gedam & Dongre, 2015) (Sani et al., 2021) . A close look at the GEO-NPCH sample reveals small peaks associated with the presence of GEO. At 3082 cm^{-1}, a peak associated with the asymmetric tension of the C—H bond for a sp^2 carbon, 1422 cm^{-1} due to the C—H deformation of Csp^2-H bond, and a strong peak at 1087 cm^{-1} as consequence of S═O group stretching can be observed.

3.4. Thermal properties of GEO-chitosan nanoparticles

Thermo Gravimetric Analysis/Differential Scanning Calorimetry (TGA/DSC) was used to evaluate the absorbed material, thermal stability, and decomposition temperatures of the GEO, NPCH, and GEO-NPCH. GEO is an extremely volatile compound that starts to evaporate even at very low temperatures, as its TGA and DSC show (Fig. 1B). This mass loss becomes more important as the temperature increases until the complete evaporation of GEO at 125 °C. Fig. 1C shows the NPCH and GEO-NPCH TGAs. NPCH shows two degradation steps, the initial step starting from the very beginning of the experiment and ending at 100 °C, and the second one starting at 170 °C up to 333 °C. The first transition corresponds to a 3.5% mass drop and is attributed to the loss of adsorbed/bound water/moisture vaporization. To confirm this fact, NPCH was heated for 1 h at 50 °C under nitrogen atmosphere and subsequently cooled down under nitrogen until room temperature was reached. After 1 h under nitrogen atmosphere, the thermogram did not show this first step of water loss (Fig. 1C, red line). The second stage of degradation was 60% weight loss, which is due to degradation of the pure chitosan biopolymer. This has been previously observed for other chitosan polymers, where the amount of moisture and the range of degradation temperatures depend on the molecular weight of the chitosan polymer (Szymańska & Winnicka, 2015). These same transitions are observed in the GEO-NPCH thermogram (Fig. 1C, blue line), coinciding in the temperature ranges. In the second transition, the mass loss was 58%, matching with the degree of NPCH decomposition. On the other hand, in the first transition, the mass loss is higher, reaching 7% and, even though the water absorbed by both particles may differ, this may indicate that this 7% loss could correspond to not only water but also GEO loss. This data was confirmed by DSC of NPCH and GEO-NPCH as shown in Fig. 1D. Similarly, to TGA, two transitions are observed in both compounds. An endothermic between −25 °C and 100 °C, and a second more complex one between 170 °C and 300 °C, combining both endothermic and exothermic processes, typical of the chitosan polymer decomposition. For the first transition, there is a considerable difference between the NPCH and GEO-NPCH evaporation enthalpies. For NPCH, an enthalpy of 145 J/g has been determined, while GEO-NPCH shows a higher value, reaching 185 J/g, which indicates that GEO-loaded nanoparticles need more energy to evaporate both water and GEO. Encapsulated GEO decomposed at higher temperature than free GEO, reflecting the improved thermal stability of GEO by encapsulation into chitosan nanoparticles.

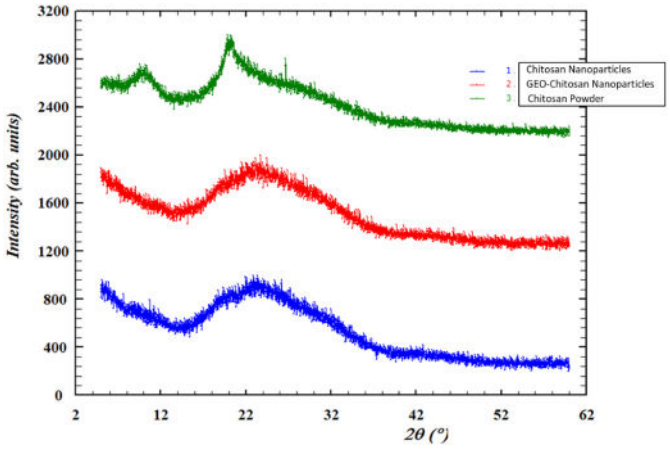

Fig. 2. X-ray diffraction pattern (XDR) of Chitosan nanoparticles, GEO-Chitosan nanoparticles, Chitosan powder.

3.5. Crystallinity of GEO-chitosan nanoparticles

Crystallographic structure of chitosan powder, NPCH, and GEO-NPCH with CH:GEO ratio of 1:0.75 were determined by XRD and are presented in Fig. 2. Chitosan powder exhibits an accused peak at 2θ around 22° showing a high degree of crystallinity (Hosseini et al., 2013). NPCH XRD patterns revealed a broad peak caused by the cross-linking reaction between chitosan and TPP, which results in the formation of an amorphous structure, reflecting the destruction of the native chitosan packing structure as described in other XDR patterns studies of Chitosan NPs (Rokhade et al., 2006; Sathiyabama & Parthasarathy, 2016).

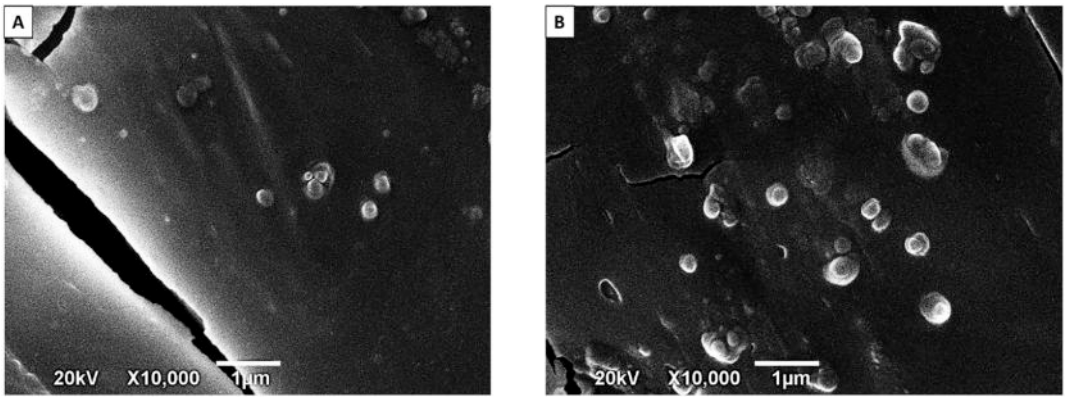

Fig. 3. SEM micrographs of A) NPCH; B) GEO-NPCH 1:0.75 ratio.

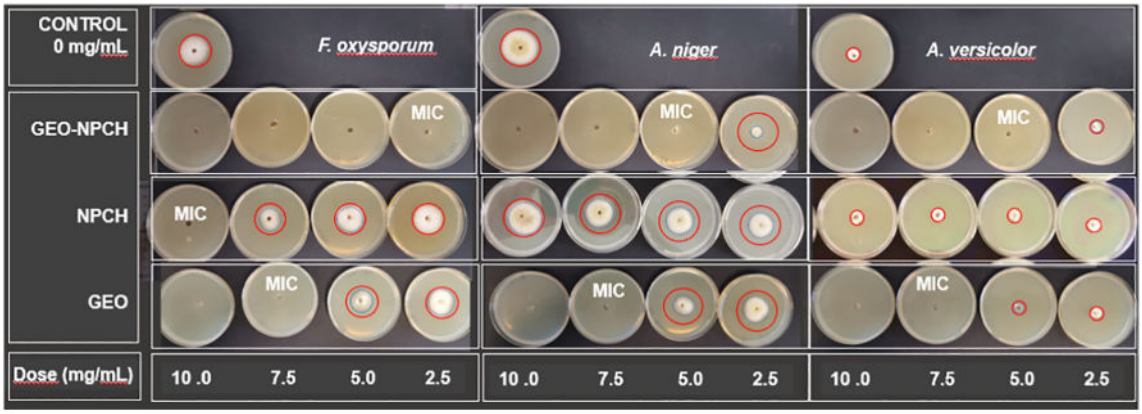

Fig. 4. MIC values of GEO-NPCH; NPCH and GEO treatments against F. oxysporum, *A. niger* and *A. versicolor* spores with prior to germination. Mycelium growth in control and treatments is notated by circles (continuous red and blue dashed lines, respectively). The figure represents one representative experiment out of three replicates.

Contrary to the study performed by Hosseini et al., regarding the encapsulation of Oregano Essential Oil (OEO), the incorporation of OEO resulted in a change in the chitosan–TPP packing structure. However, in our case, the inclusion of GEO to chitosan NPs did not produce changes in its crystallinity compared to NPCH.

3.6. Morphological characterization of GEO-chitosan nanoparticles

SEM micrograph was performed to evaluate the morphological and superficial characteristics of NPCH and GEO-NPCH. SEM imaging is an effective method to provide the surface morphology and more accurate size and size distribution. SEM imaging in Fig. 3 shows a spherical nanoparticle in both cases, with size diameter of less than 200 nm in the case of NPCH and less than 400 nm in GEO-NPCH in most NPs, confirming the increase of size after GEO encapsulation. Also, these images are in agreement with sizes obtained by DLS measurement and PDI values, where swelling and aggregation in NPs formed during dispersion in water suspension is observed. This has also been shown in previous reports i.e. eugenol encapsulated in chitosan nanoparticles where a higher both size and PDI values were obtained in DLS than TEM images due to swelling and aggregation of nanoparticles in water dispersions (Woranuch & Yoksan, 2013). The same effects were also observed in formulations with carvacrol (Keawchaoon & Yoksan, 2011).

Table 2
MIC values of GEO-NPCH; NPCH and GEO treatments against F. oxysporum, *A. niger* and *A. versicolor* spores after germination. Treatments were performed in liquid PDB medium multiwell plates at lower doses. Data was generated as a result of three independent experiments.

	Germinated spore treatment (mg/mL)			
Fungi	NPCH (mg/mL)	GEO NPCH (mg/mL)	GEO (mg/mL)	TB (mg/mL)
F.oxysporum	3.33	1.11	1.66	>3.33
A.niger	1.11	0.37	0.56	0.11
A.versicolor	>3.33	3.33	15.00	3.33

3.7. Antifugal properties of geo-NPCH

Economically important cereal diseases including *Blumeria graminis*, *Puccina recondita*, *Puccinia graminis*, *Puccina striiformis*, *Septoria tritici* and *Septoria nodorum*, as well as *Fusarium* have been reported (Rózewicz et al., 2021).

Fusarium head blight is the most important disease affecting wheat cultivation, while other fungi from the genus *Fusarium*, can also cause a number of other diseases: seedling wilt, root rot, or take-all disease. In addition to the different cereal diseases caused by the mentioned fungi, there are fungi that cause losses of grain during storage and after harvest. A recent study showed that cereal grains were infested to various degrees during storage. A total of 21 different fungi, namely *Alternaria alternata, Penicillium sp, Aspergillus niger, A. flavus, Curvularia lunata, Rhizopus stolonifer, Fusarium oxysporum* and *Mucus* species were isolated. *Aspergillus* was the most frequently isolated fungus followed by *Aspergillus niger, A. flavus, Aspergillus versicolor, Aspergillus parasiticus, Aspergillus ochraceus*, were frequently isolated from the grains (Varsha bhalerao & Ashok chavan, 2008).

The most widely used method to protect cereal against pathogens is

Table 3
Percentage of seed germination from barley, wheat and oat after different treatments.

Cereal/treatment	Germinationn %	Cereal/treatment	Germinationn %	Cereal/treatment	Germination %
Barley/NT	98.7 ± 0.58	Wheat/NT	82.0 ± 1.15	Oat/NT	95.3 ± 0.58
Barley/NPCH	98.3 ± 0.79	Wheat/NPCH	87.7 ± 1.52	Oat/NPCH	98.7 ± 1.53
Barley/GEO-NPCH	98.3 ± 0.84	Wheat/GEO-NPCH	90.3 ± 1.53	Oat/GEO-NPCH	99.7 ± 0.47
Barley/TB	98.7 ± 0.42	Wheat/TB	93.0 ± 5.20	Oat/TB	95.3 ± 0.63

NT: Non treated.

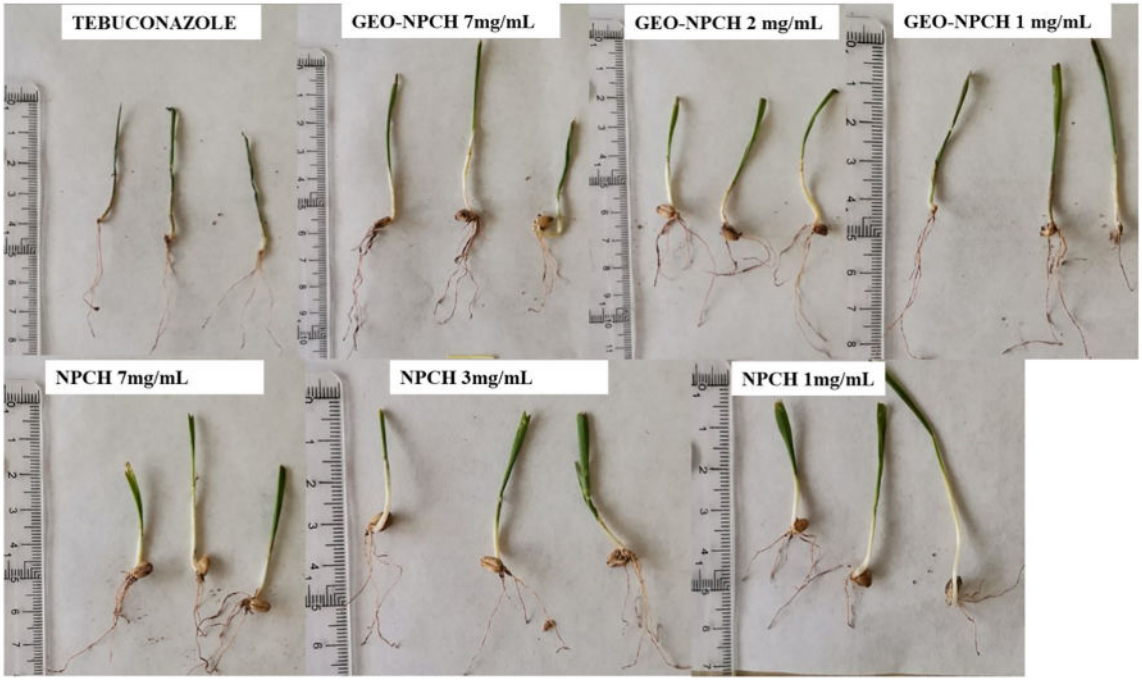

Fig. 5. Wheat seedlings 15 days aftersowing; GEO-NPCH 7 mg/mL (0.7 mg/mL of pure GEO), GEO-NPCH 2 mg/mL (0.2 mg/mL of pure GEO), GEO-NPCH 1 mg/mL (0.1 mg/mL of pure GEO).

fungicide application. This practice has led to an increase in resistance to the different fungicides employed. The use of chemical plant protection is also associated with environmental contamination by delivering active substances that have an adverse effect on air, water, soil, or living organisms. The search for alternative and greener methods to control fungal pathogens in cereal diseases, post-harvest and storage, lead us to assay different concentrations of nanoparticles against species from *Fusarium* and *Aspergillus*.

The antifungal activity of NPCH, GEO and GEO-NPCH against *Fusarium* and *Aspergillus* was evaluated calculating MIC values in two different scenarios. First, the antifungal effect of GEO-NPCH, NPCH and GEO was tested against the different spores prior its germination (Fig. 4).

NPCH MIC value against *F. oxysposum* growth was 10.0 mg/mL, according to the assayed concentrations, whereas no inhibition was observed in the other two species. Lower MIC values were obtained by GEO treatment reaching 7,5 mg/mL against all the fungi tested. In contrast, GEO-NPCH treatment was more effective against all of them, especially against *F. oxysporum* showing an MIC of 2.5 mg/mL followed by *A. niger* and *A. versicolor* with an MIC of 5.0 mg/mL.

Alternatively, MIC evaluation of TB treatment against *Fusarium* and *Aspergillus* spores required lower doses ranging from 0,115 m/mL to 2 mg/mL. Pure TB at commercial dose inhibited the germination of spores from the assayed fungi with concentrations lower than 0.5 mg/mL for *A. niger* and *A. versicolor*. The commercial recommendation of pure TB was 9.0 mg/mL, at this dose negative effects on germination and growth of the seeds were observed as compared to NPCH or GEO-NPCH. By contrast, seeds treated by nanoparticles did not show any controversial effects, indeed plantlets showed greater height compared to the control, thus indicating a possible effect in promoting growth properties.

By encapsulating the GEO into chitosan the MIC values went down, resulting in a 10% decrease in the amount of the GEO necessary to generate the same inhibiting action against the fungi tested.

The antimycotic properties of the nanoparticles were evaluated on mycelia after spore germination (Table 2). This strategy aims to evaluate the effectiveness of the treatment once the fungus starts to attack the crop. The obtained MIC values were lower in comparison with the MICs obtained on spores, a result which was expected, since cell wall spores are thicker than the hyphae. For instance, *A. niger* was the most sensitive fungus and showed an MIC value for GEO-NPCH of 0.33 mg/mL. When using the same treatment against spores the value was 5.0 mg/mL. The same behaviour was observed using TB and GEO with an MIC value of 0.11 mg/mL and 0.5 mg/mL, respectively. On the other hand *F. oxysporum* showed the same patterns as *A. niger* using NPCH, GEO NPCH and GEO, although it was less sensitive to TB when hyphae were treated, displaying an MIC value >3.33 mg/mL. Finally, *A. versicolor* displayed an MIC value of 15.0 mg/mL when treated by GEO although its encapsulation increased the antifungal effect significantly, lowering its MIC to 3.33 mg/mL.

3.8. Effects of GEO-NPCH in dressed seeds

To estimate the effect of GEO-NPCH on different types of seeds, a batch composed of 100 seeds of wheat, oat and barley was evaluated to

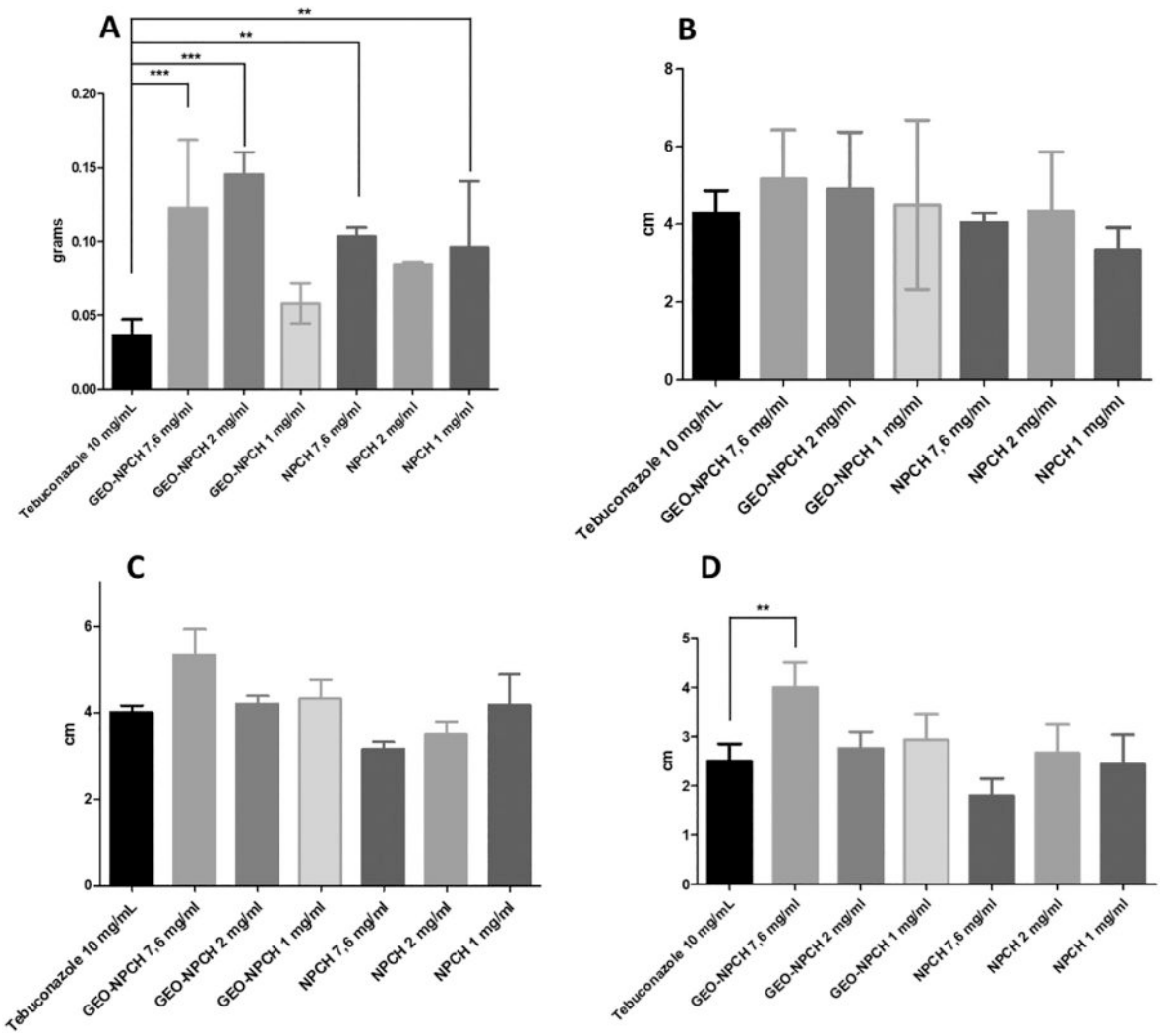

Fig. 6. Evaluation of morphological changes after wheat seed treatment; A) Total weight (grams); B) Root length; C) Total leave length; D) Green part length of Wheat seedling with 15 days. Asterisks indicate statistical significance of differences between the different treatments and Tebuconazole 10 mg/mL using one-way ANOVA and Dunnet's Multiple Comparisons test (*- $p < 0.05$, **-$p < 0.01$ and ***-$p < 0.001$).

determine the germination rate after 7 and 15 days of treatment using GEO-NPCH, with TB and non-treated seeds as control (Table 3). After 7 days, the highest germination rate was observed in barley, and all the treatments achieved values close to 99% of germination. The non-treated seeds showed similar values. In oat, GEO-NPCH showed a higher germination rate, reaching 99.7% compared to TB, displaying an effect on germination equal to those obtained on non-treated seeds. On the other hand, non-treated wheat seeds showed a germination rate of 82% while seeds treated by TB and GEO-NPCH reached higher germination rates with 93.0% and 90.3% respectively.

In contrast, the batch of seeds evaluated after 15 days (Fig. 5.) showed different morphological characteristics depending on the treatment used. The seeds treated with TB consumed all energy resources, as occurs in other species such as maize, where conventional treatments with TB produces reductions in shoot height, shoot fresh weight and fresh root, pointing out that the suppression of maize emergence induced by TB was exponentially dose dependent (Yang et al., 2014). Also, data presented in Fig. 6A showed that GEO-NPCH at 7.6 mg/mL and 2 mg/mL doses have a significantly greater total weight ($p < 0.05$) than TB seeds at 10 mg/mL of pure TB. NPCH treatments also displayed a more significative increase ($p < 0.05$) in total weight than TB seeds (Fig. 6B). The length of roots was significantly ($P < 0.05$) increased by treatment with GEO-NPCH compared to the untreated control, TB and NPCH.

Similarly, GEO-NPCH at 7 mg/mL shows an increase in total leaf length (Fig. 6C) and significative growth ($p < 0.05$) of green parts in leaves (Fig. 6 D) in comparison to the other treatments, hence suggesting that GEO-NPCH may promote germination and growth of wheat seeds in field conditions. Secondary metabolites can affect seed germination and plant productivity since essential oils contain bioactive compounds, such as monoterpenes and sesquiterpenoids, which belong to the allelochemicals and are involved in many metabolic and ecological processes. Low doses of allelochemicals promote growth and enhance jasmonic acid-mediated dormancy release of target crops by stimulating mild stress responses This phenomenon is known as seed priming, which involves seed treatment with transient stressing agents during the first hydration phase of the priming process within embryos, leading to a stress memory and more efficient adaptation to subsequent episodes of stress. (Dudai et al., 2004; Rentzsch et al., 2012) In previous findings, coating seeds with essential oil activated seed germination and growth promotion derived from the beneficial effect of the transient acidification of seed endosperms and embryos induced by the monoterpenes present in the Eos, leading to an increased permeability of membranes, and the generation of ROS (Ben-Jabeur et al., 2019). The acidification of seed endosperm and embryo produces multiple effects such as altering the inhibitory effect of ABA, acidifying the cytosol, and stimulating the

electrogenic proton pump favouring the germination rates, cell enlargement, and elongation of seedling (Blankenship et al., 2014; Brummer et al., 1984), solubilizing starch, and the mobilization of macronutrient elements during germination (Hamabata et al., 1988); or weakening of membrane barriers of the endosperm cells, allowing a larger uptake of water leading to the interruption of dormancy, and promotion of germination and growth. Furthermore the use of chitosan as raw material to generate the nanoparticles leads to the accumulation of phytoalexins, pathogen-related proteins (PR) and proteinase inhibitors, lignin synthesis, and callose formation producing an invigorating effect in treated plants (Hadrami et al., 2010). Our findings coincide with previous results, in which seed treatments modify emergence characteristics of seeds planted in fields. On the other hand, very low rates of chitosan seed treatment may stimulate shoot growth as described in wheat (Li et al., 2019) and chickpea (Sathiyabama & Parthasarathy, 2016).

4. Conclusion

The fungicide and fungistatic activities of essential oils, along with knowledge of their traditional and new uses, together with the growing literature on their mechanisms of action, have made them an attractive alternative for synthetic fungicides. The successful use of essential oil as a fungicide is probably the effect of the synergy of multiple compounds, making them more effective against plant pathogenic fungi. Our data revealed that the combination of GEO and NPCH increases the fungicide capacity of the GEO decreasing of MIC of 7.5 mg/mL (pure GEO) to 2.5 mg/mL (GEO-NPCH) in *F. oxysporum* with 10% of GEO in this dose (0.25 mg/mL pure GEO). This activity is similar to the TB, however the use of TB decreases wheat seed germination while coating seeds with GEO-NCPH enhanced seed germination and seedling development. Overall, coating seeds with GEO-NCPH is a promising alternative approach to overcome fungal disease and to preserve plant fitness for greater yield potential. Moreover, another advantage is that the GEO-NPCH is not harmful and, because of its natural origin, will be more likely accepted by consumers than synthetic agents. Furthermore, essential oil and plant extracts in general degrade more rapidly than most chemical fungicides and are eco- friendly and less likely to kill beneficial fungi than synthetic fungicides with longer environmental retention.

Acknowledgment

Our thanks to Alejandro Santiago González, curator of the Botanical Garden of Castilla-La Mancha for providing vegetal samples, to Javier Argandoña for his technical assistance and to K.A. Walsh for language revision.This work was supported by contract number 200360UCTR from Candelo biotech by Cereales Candelo S.L. EN was supported by the Universidad Castilla-La Mancha through a grant " Contratos de investigadores posdoctorales para la excelencia científica en el desarrollo del plan propio de I+D+I " from University of Castilla-La Mancha. We thank the unidad de prestación de servicios at IER-uclm for providing access to SEM facilities

References

Ang, F., .I., ueangl, X., Hu, F., Ei, C., & L, I. (2009). Structural Characterization of Nanoparticles Loaded with Garlic Essential Oil and Their Insecticidal Activity against Tribolium castaneum (Herbst) (Coleoptera : Tenebrionidae). *Agric. Food Chem., 57*, 10156–10162. https://doi.org/10.1021/jf9023118

Ashra, B., Rashidipour, M., Marzban, A., & Soroush, S. (2019). Mentha piperita essential oils loaded in a chitosan nanogel with inhibitory effect on biofilm formation against S . mutans on the dental surface. *Carbohydrate Polymers, 212*(December 2018), 142–149. https://doi.org/10.1016/j.carbpol.2019.02.018

Ben-Jabeur, M., Vicente, R., López-Cristoffanini, C., Alesami, N., Djébali, N., Gracia-Romero, A., Serret, M. D., López-Carbonell, M., Araus, J. L., & Hamada, W. (2019). A novel aspect of essential oils: Coating seeds with thyme essential oil induces drought resistance in wheat. *Plants, 8*(10). https://doi.org/10.3390/plants8100371

Benkeblia, N. (2004). Antimicrobial activity of essential oil extracts of various onions (Allium cepa) and garlic (Allium sativum). *LWT - Food Science and Technology, 37*(2), 263–268. https://doi.org/10.1016/j.lwt.2003.09.001

Bittelli, M., Flury, M., Campbell, G. S., & Nichols, E. J. (2001). Reduction of transpiration through foliar application of chitosan. *Agricultural and Forest Metereology, 107*, 167–175.

Blankenship, J. O., Smith, D. R., Blankenship, J., & Smith, D. R. (2014). Breaking seed dormancy in Parry's clover by acid treatment. *Journal of Range Management, 20*(1).

Brauer, V. S., Rezende, C. P., Pessoni, A. M., De Paula, R. G., Rangappa, K. S., Nayaka, S. C., Gupta, V. K., & Almeida, F. (2019). Antifungal agents in agriculture: Friends and foes of public health. *Biomolecules, 9*(10), 1–21. https://doi.org/10.3390/biom9100521

Brummer, B., Felle, H., & Parish, R. W. (1984). Evidence that acid solutions induce plant cell elongation by acidifying the cytosol and stimulating the proton pump. *FEBS Letters, 174*(2), 223–227. https://doi.org/10.1016/0014-5793(84)81162-X

Çakır, M. A., Icyer, N. C., & Tornuk, F. (2020). Optimization of production parameters for fabrication of thymol-loaded chitosan nanoparticles. *International Journal of Biological Macromolecules, 151*, 230–238. https://doi.org/10.1016/j.ijbiomac.2020.02.096

Chun, S. C., & Chandrasekaran, M. (2019). Chitosan and chitosan nanoparticles induced expression of pathogenesis-related proteins genes enhances biotic stress tolerance in tomato. *International Journal of Biological Macromolecules, 125*, 948–954. https://doi.org/10.1016/j.ijbiomac.2018.12.167

D'agostino, M., Tesse, N., Frippiat, J. P., Machouart, M., & Debourgogne, A. (2019). Essential oils and their natural active compounds presenting antifungal properties. *Molecules, 24*(20). https://doi.org/10.3390/molecules24203713

Danaei, M., Dehghankhold, M., Ataei, S., Hasanzadeh Davarani, F., Javanmard, R., Dokhani, A., Khorasani, S., & Mozafari, M. R. (2018). Impact of particle size and polydispersity index on the clinical applications of lipidic nanocarrier systems. *Pharmaceutics, 10*(2), 1–17. https://doi.org/10.3390/pharmaceutics10020057

Das, S., Singh, V. K., Dwivedy, A. K., Chaudhari, A. K., Upadhyay, N., Singh, P., Sharma, S., & Dubey, N. K. (2019). Encapsulation in chitosan-based nanomatrix as an efficient green technology to boost the antimicrobial, antioxidant and in situ efficacy of Coriandrum sativum essential oil. *International Journal of Biological Macromolecules, 133*, 294–305. https://doi.org/10.1016/j.ijbiomac.2019.04.070

Delan, W. K., Zakaria, M., Elsaadany, B., ElMeshad, A. N., Mamdouh, W., & Fares, A. R. (2020). Formulation of simvastatin chitosan nanoparticles for controlled delivery in bone regeneration: Optimization using Box-Behnken design, stability and in vivo study. *International Journal of Pharmaceutics, 577*(September 2019), Article 119038. https://doi.org/10.1016/j.ijpharm.2020.119038

Dudai, N., Ben-Ami, M., Chaimovich, R., & Chaimovitsh, D. (2004). Essential oils as allelopathic agents: Bioconversion of monoterpenes by germinating wheat seeds. *Acta Horticulturae, 629*, 505–508. 10.17660/ActaHortic.2004.629.65.

Fakhreddin, S., Zandi, M., Rezaei, M., & Farahmandghavi, F. (2013). Two-step method for encapsulation of oregano essential oil in chitosan nanoparticles : Preparation, characterization and in vitro release study. *Carbohydrate Polymers, 95*(1), 50–56. https://doi.org/10.1016/j.carbpol.2013.02.031

Fisher, M. C. Henk, Briggs, D. A., Brownstein, C. J., Madoff, J. S., McCraw, L. C., & Gurr, S. L. (2012). Emerging fungal threats to animal, plant and ecosystem health. *484*, 186–194. https://doi.org/10.1038/nature10947

Feyzioglu, G. C., & Tornuk, F. (2016). Development of chitosan nanoparticles loaded with summer savory (Satureja hortensis L.) essential oil for antimicrobial and antioxidant delivery applications. *LWT - Food Science and Technology, 70*, 104–110. https://doi.org/10.1016/j.lwt.2016.02.037

Gardes, M., Bruns, T. D., & Pathology, P. (1993). ITS primers with enhanced specificity for basidiomycetes -Application to the identification of mycorrhizae and rusts. *Molecular Ecology*, 113–118.

Gedam, A. H., & Dongre, R. S. (2015). Adsorption characterization of Pb(ii) ions onto iodate doped chitosan composite: Equilibrium and kinetic studies. *RSC Advances, 5*(67), 54188–54201. https://doi.org/10.1039/c5ra09899h

Hadidi, M., Pouramin, S., Adinepour, F., Haghani, S., & Jafari, S. M. (2020). Chitosan nanoparticles loaded with clove essential oil: Characterization, antioxidant and antibacterial activities. *Carbohydrate Polymers, 236*(February), Article 116075. https://doi.org/10.1016/j.carbpol.2020.116075

Hadrami, A. E., Adam, L. R., Hadrami, I. E., & Daayf, F. (2010). Chitosan in plant protection. *Marine Drugs, 8*, 968–987. https://doi.org/10.3390/md8040968

Hamabata, A., García-Maya, M., Romero, T., & Bernal-Lugo, I. (1988). Kinetics of the acidification capacity of aleurone layer and its effect upon solubilization of reserve substances from starchy endosperm of wheat. *Plant Physiology, 86*(3), 643–644. https://doi.org/10.1104/pp.86.3.643

Hasheminejad, N., Khodaiyan, F., & Safari, M. (2019). Improving the antifungal activity of clove essential oil encapsulated by chitosan nanoparticles. *Food Chemistry, 275*(April 2018), 113–122. https://doi.org/10.1016/j.foodchem.2018.09.085

Hasheminejad, N., Khodaiyan, F., & Safari, M. (2019). Improving the antifungal activity of clove essential oil encapsulated by chitosan nanoparticles. *Food Chemistry, 275*(August 2018), 113–122. https://doi.org/10.1016/j.foodchem.2018.09.085

Hosseini, S. F., Zandi, M., Rezaei, M., & Farahmandghavi, F. (2013). Two-step method for encapsulation of oregano essential oil in chitosan nanoparticles: Preparation, characterization and in vitro release study. *Carbohydrate Polymers, 95*(1), 50–56. https://doi.org/10.1016/j.carbpol.2013.02.031

Hosseinnejad, M., & Mahdi, S. (2016). International journal of biological macromolecules evaluation of different factors affecting antimicrobial properties of chitosan. *International Journal of Biological Macromolecules, 85*, 467–475. https://doi.org/10.1016/j.ijbiomac.2016.01.022

Hu, Q., & Luo, Y. (2016). Polyphenol-chitosan conjugates: Synthesis, characterization, and applications. *Carbohydrate Polymers, 151*, 624–639. https://doi.org/10.1016/j.carbpol.2016.05.109

Kalagatur, N. K., Ghosh, O. S. N., & Sundararaj, N. (2018). Antifungal activity of chitosan nanoparticles encapsulated with Cymbopogon martinii essential oil on plant pathogenic fungi Fusarium graminearum. *Frontiers in Pharmacology, 9*(June), 1–13. https://doi.org/10.3389/fphar.2018.00610

Kamkar, A., Molaee-aghaee, E., Khanjari, A., Akhondzadeh-basti, A., Noudoost, B., Shariatifar, N., Alizadeh, M., & Soleimani, M. (2021). *342*(January).

Kananont, N., Pichyangkura, R., Chanprame, S., & Chadchawan, S. (2010). Chitosan specificity for the in vitro seed germination of two dendrobium orchids (Aasparagales: Orchidaceae). *Scientia Horticulturae, 124*(2), 239–247. https://doi.org/10.1016/j.scienta.2009.11.019

Keawchaoon, L., & Yoksan, R. (2011). Preparation, characterization and in vitro release study of carvacrol-loaded chitosan nanoparticles. *Colloids and Surfaces B: Biointerfaces, 84*(1), 163–171. https://doi.org/10.1016/j.colsurfb.2010.12.031

Kumar, A., Singh, P. P., & Prakash, B. (2020). Unravelling the antifungal and anti-a fl atoxin B 1 mechanism of chitosan nanocomposite incorporated with Foeniculum vulgare essential oil. *Carbohydrate Polymers, 236*(January), Article 116050. https://doi.org/10.1016/j.carbpol.2020.116050

Li, R., He, J., Xie, H., Wang, W., Kumar, S., Sun, Y., Hu, J., & Yin, H. (2019). Effects of chitosan nanoparticles on seed germination and seedling growth of wheat (Triticum aestivum L.). *International Journal of Biological Macromolecules, 126*, 91–100. https://doi.org/10.1016/j.ijbiomac.2018.12.118

Lopez-Antia, A., Ortiz-Santaliestra, M. E., Mougeot, F., Camarero, P. R., & Mateo, R. (2021). Birds feeding on tebuconazole treated seeds have reduced breeding output. *Environmental Pollution, 271*, Article 116292. https://doi.org/10.1016/j.envpol.2020.116292

Mahizan, N. A., Yang, S. K., Moo, C. L., Song, A. A. L., Chong, C. M., Chong, C. W., Abushelaibi, A., Erin Lim, S. H., & Lai, K. S. (2019). Terpene derivatives as a potential agent against antimicrobial resistance (AMR) pathogens. *Molecules, 24*(14), 1–21. https://doi.org/10.3390/molecules24142631

Marín, P., de Ory, A., Cruz, A., Magan, N., & González-Jaén, M. T. (2013). Potential effects of environmental conditions on the efficiency of the antifungal tebuconazole controlling Fusarium verticillioides and fusarium proliferatum growth rate and fumonisin biosynthesis. *International Journal of Food Microbiology, 165*(3), 251–258. https://doi.org/10.1016/j.ijfoodmicro.2013.05.022

Matshetshe, K. I., Parani, S., Manki, S. M., & Oluwafemi, O. S. (2018). Preparation, characterization and in vitro release study of β-cyclodextrin/chitosan nanoparticles loaded Cinnamomum zeylanicum essential oil. *International Journal of Biological Macromolecules, 118*, 676–682. https://doi.org/10.1016/j.ijbiomac.2018.06.125

Muzzarelli, R. A. A., Muzzarelli, C., Tarsi, R., Miliani, M., Gabbanelli, F., & Cartolari, M. (2001). Fungistatic activity of modified chitosans against Saprolegnia parasitica. *Biomacromolecules, 2*, 165–169.

Nazzaro, F. (2017). In *Essential oils and antifungal activity* (pp. 1–20). https://doi.org/10.3390/ph10040086

Niza, E., Božik, M., Bravo, I., Clemente-Casares, P., Lara-Sanchez, A., Juan, A., Klouček, P., & Alonso-Moreno, C. (2020). PEI-coated PLA nanoparticles to enhance the antimicrobial activity of carvacrol. *Food Chemistry, 328*(February). https://doi.org/10.1016/j.foodchem.2020.127131

Palmero, D., Rubio-moraga, A., Galvez-patón, L., Nogueras, J., Abato, C., Gómez-gómez, L., & Ahrazem, O. (2014). Pathogenicity and genetic diversity of Fusarium oxysporum isolates from corms of Crocus sativus. *Industrial Crops & Products, 61*, 186–192. https://doi.org/10.1016/j.indcrop.2014.06.051

Rabea, E. I., Stevens, C. V., Smagghe, G., & Steurbaut, W. (2003). Chitosan as antimicrobial agent: Applications and mode of action. *Biomacromolecules, 4*(6), 1457–1465.

Rentzsch, S., Podzimska, D., Voegele, A., Imbeck, M., Müller, K., Linkies, A., & Leubner-Metzger, G. (2012). Dose- and tissue-specific interaction of monoterpenes with the gibberellin-mediated release of potato tuber bud dormancy, sprout growth and induction of α-amylases and β-amylases. *Planta, 235*(1), 137–151. https://doi.org/10.1007/s00425-011-1501-1

Rokhade, A. P., Agnihotri, S. A., Patil, S. A., Mallikarjuna, N. N., Kulkarni, P. V., & Aminabhavi, T. M. (2006). Semi-interpenetrating polymer network microspheres of gelatin and sodium carboxymethyl cellulose for controlled release of ketorolac tromethamine. *Carbohydrate Polymers, 65*(3), 243–252. https://doi.org/10.1016/j.carbpol.2006.01.013

Rózewicz, M., Wyzinska, M., & Grabinski, J. (2021). The most important fungal diseases of cereals — Problems and. *Agronomy, 11*(714).

Rubio-moraga, Á., Gómez-gómez, L., & Trapero, A. (2013). Saffron corm as a natural source of fungicides : The role of saponins in the underground. *Industrial Crops & Products, 49*, 915–921. https://doi.org/10.1016/j.indcrop.2013.06.029

Sani, M. A., Tavassoli, M., Hamishehkar, H., & McClements, D. J. (2021). Carbohydrate-based films containing pH-sensitive red barberry anthocyanins: Application as biodegradable smart food packaging materials. *Carbohydrate Polymers, 255*(October 2020), Article 117488. https://doi.org/10.1016/j.carbpol.2020.117488

Sathiyabama, M., & Parthasarathy, R. (2016). Biological preparation of chitosan nanoparticles and its in vitro antifungal efficacy against some phytopathogenic fungi. *Carbohydrate Polymers, 151*, 321–325. https://doi.org/10.1016/j.carbpol.2016.05.033

Somrani, M., Inglés, M. C., Debbabi, H., Abidi, F., & Palop, A. (2020). Garlic, onion, and cinnamon essential oil anti-biofilms' effect against listeria monocytogenes. *Foods, 9*(5), 1–12. https://doi.org/10.3390/foods9050567

Szymańska, E., & Winnicka, K. (2015). Stability of chitosan - A challenge for pharmaceutical and biomedical applications. *Marine Drugs, 13*(4), 1819–1846. https://doi.org/10.3390/md13041819

Tavassoli, M., Alizadeh, M., Khezerlou, A., Ehsani, A., & Julian, D. (2021). Multifunctional nanocomposite active packaging materials: Immobilization of quercetin, lactoferrin, and chitosan nanofiber particles in gelatin films. *Food Hydrocolloids, 118*(March), Article 106747. https://doi.org/10.1016/j.foodhyd.2021.106747

Thuy, B. T. P., My, T. T. A., Hai, N. T. T., Hieu, L. T., Hoa, T. T., Thi Phuong Loan, H., … Nhung, N. T. A. (2020). Investigation into SARS-CoV-2 resistance of compounds in garlic essential oil. *ACS Omega, 5*(14), 8312–8320. https://doi.org/10.1021/acsomega.0c00772

Valdivieso-Ugarte, M., Gomez-Llorente, C., Plaza-Díaz, J., & Gil, Á. (2019). Antimicrobial, antioxidant, and immunomodulatory properties of essential oils: A systematic review. *Nutrients, 11*(11), 1–29. https://doi.org/10.3390/nu11112786

Varsha bhalerao, A., & Ashok chavan, M. (2008). Isolation of filamentous fungi in post-harvest cereal grain during the storage and their effect in seed health. *International Journal of Advanced Research, 5*(8), 2171–2177. https://doi.org/10.21474/IJAR01/5283

Woranuch, S., & Yoksan, R. (2013). Eugenol-loaded chitosan nanoparticles : I. Thermal stability improvement of eugenol through encapsulation. *Carbohydrate Polymers, 96*(2), 578–585. https://doi.org/10.1016/j.carbpol.2012.08.117

Yang, D., Wang, N., Yan, X., Shi, J., Zhang, M., Wang, Z., & Yuan, H. (2014). Microencapsulation of seed-coating tebuconazole and its effects on physiology and biochemistry of maize seedlings. *Colloids and Surfaces B: Biointerfaces, 114*, 241–246. https://doi.org/10.1016/j.colsurfb.2013.10.014